Liquid-Solid Boundaries Dominate Activity of CO_2 Reduction on Gas-Diffusion Electrodes

Nesbitt, Nathan T.; Burdyny, Thomas; Salvatore, Danielle; Bohra, Divya; Kas, Recep; Smith, Wilson A.

DOI
10.1021/acscatal.0c03319

Publication date
2020

Document Version
Accepted author manuscript

Published in
ACS Catalysis

Liquid-solid boundaries dominate activity of CO_2 reduction on gas-diffusion electrodes

Nathan T. Nesbitt,[a] Thomas Burdyny,[b] Hunter Simonson,[c,d] Danielle Salvatore,[c,d] Divya Bohra,[b] Recep Kas,[a,d] Wilson A. Smith*[a,b,c,d].*

a. Materials and Chemical Science and Technology (MCST) Directorate, National Renewable Energy Laboratory, Golden, CO 80401, United States of America.

b. Materials for Energy Conversion and Storage, Department of Chemical Engineering, Delft University of Technology, 2629 HZ Delft, The Netherlands.

c. Department of Chemical and Biological Engineering, University of Colorado Boulder, Colorado 80303, United States

d. Renewable and Sustainable Energy Institute (RASEI), University of Colorado Boulder, Colorado 80303, United States.

KEYWORDS (Word Style "BG_Keywords"). Gas-diffusion electrode, triple-phase boundary, double-phase boundary, CO_2 reduction, CO_2 electrolysis.

ABSTRACT:

Electrochemical CO_2 electrolysis to produce hydrocarbon fuels or material feedstocks offers a renewable alternative to fossilized carbon sources. Gas diffusion electrodes (GDEs), composed of solid electrocatalysts on porous supports positioned near the interface of a conducting electrolyte and CO_2 gas, have been able to demonstrate the substantial current densities needed for future commercialization. These higher reaction rates have often been ascribed to the presence of a three-phase interface, where solid, liquid, and gas provide electrons, water, and CO_2, respectively. Conversely, mechanistic work on electrochemical reactions implicates a fully two-phase reaction interface, where gas molecules reach the electrocatalyst's surface by dissolution and diffusion through the electrolyte. Because the discrepancy between an atomistic three-phase vs. two-phase reaction has substantial implications for the design of catalysts, gas-diffusion layers and cell architectures, the nuances of nomenclatures and governing phenomena surrounding the three-phase-region require clarification. Here, we outline the macro, micro and atomistic phenomena occurring within a gas-diffusion electrode to provide a focused discussion on the architecture of the often-discussed three-phase region for CO_2 electrolysis. From this information, we comment on the outlook for the broader CO_2 electro-reduction GDE cell architecture.

TEXT:

1. Introduction

The electrochemical reduction of CO_2 (CO_2R) to make high value chemicals, such as fuels or material feedstocks, offers a means to lower net CO_2 emissions into the atmosphere. To reduce costs and maximize this technology's impact, high current densities are needed to balance the cost of infrastructure over the volume of product. Commercial viability is estimated to require over 200 mA cm^{-2},[1,2] while even higher current densities may be needed to minimize the total electrocatalyst surface area and for products that require > $2H^+/e^-$.[3] To achieve these industrially relevant operating conditions, supporting electrocatalysts on hydrophobic gas diffusion layers (GDLs) to make gas diffusion electrodes (GDEs) has enabled cell designs capable of reaching higher current densities than the conventional aqueous H-cells traditionally used in the CO_2R literature.

In the classical H-cell configuration, two solid electrodes are immersed in a liquid electrolyte. The electrolyte is typically aqueous, often 0.1 to 1 M $KHCO_3$, and is saturated by CO_2 gas.[4] The solubility limit of CO_2 at standard temperature and pressure (STP) (20 ºC, 1 atm) is approximately 33 mM, and the diffusion rate of CO_2 is slow enough to limit the current density to approximately 35-100 mA cm^{-2} (lower for C1 products, higher for C2).[5] Here, the reaction of CO_2 indisputably occurs at the liquid-solid interface of the electrolyte and the electrocatalyst.

GDE-based cells have three common configurations: microfluidic cells,[6] hybrid cells,[7] and zero-gap cells,[8,9] respectively characterized by a flowing liquid electrolyte between the cathode and anode (Figure S1a), flowing liquid electrolyte between the cathode and anode separated by a membrane (Figure 1a, S1b), and a cathode and anode pressed directly against a membrane with no macroscopic gap for liquid flow (Figure S1c). The GDL, often made of a macroporous

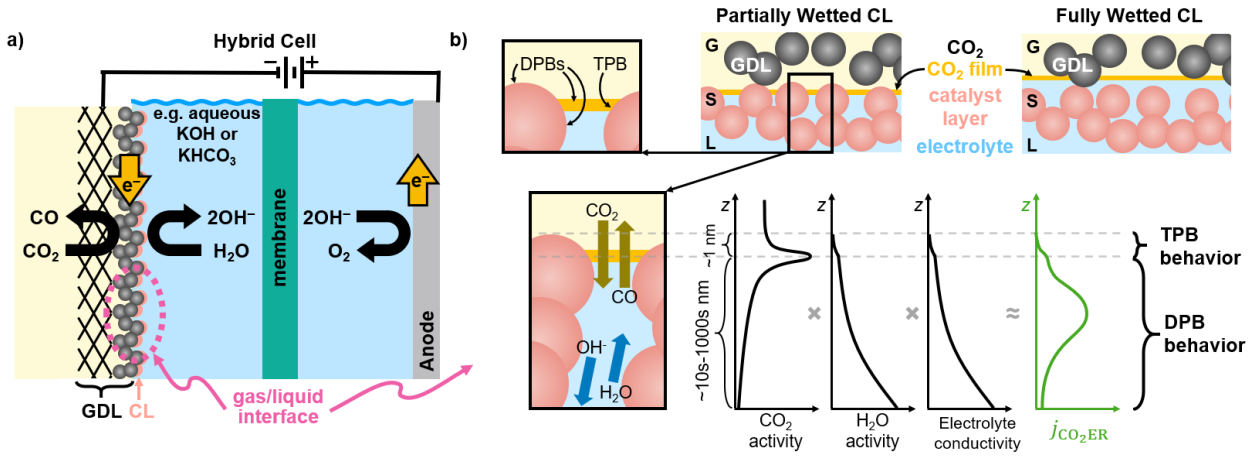

Figure 1. (a) Schematic (not to scale) showing the general gas diffusion electrode (GDE) cell architecture for a catalyst layer (CL) that produces CO, with a gas-diffusion layer (GDL) that is hydrophobic to mediate gas transport. (b) (top-left) Pictorial representation of a triple-phase boundary (TPB) in a GDE if the CL was partially wetted, and (top-right) of the exclusive double-phase boundary (DPB) if the CL was fully wetted, (bottom) magnified view of a partially wetted pore showing the direction of diffusion of reactants and products; note: no attempt was made here to speculate at the meniscus shapes. Plots depict qualitative change in CO_2 activity, H_2O activity, electrolyte conductivity, and the resulting CO_2R current density as predicted by later sections of this perspective.

carbon paper topped by a microporous layer (MPL) of PTFE and carbon particles, is hydrophobic and provides a barrier to liquid, allowing for it to be filled by gaseous CO_2. The catalyst layer (CL), often made of a metal film[7] or of catalyst particles mixed with carbon particles and a polymer binder,[10] provides the interface between the electrocatalyst and reactants. The polymer binder is typically either ion and water conducting ionomers, or hydrophobic PTFE. Such GDE-based cells have been able to achieve current densities which are substantially higher than H-cell architectures, such as 750 mA cm^{-2} with 63% Faradaic efficiency (F.E.) for ethylene (C_2H_4) with a Cu catalyst,[7] 350 mA cm^{-2} with 100% F.E. for CO with a Ag catalyst,[11] 200 mA cm^{-2} with 84% F.E. for CO with a non-noble Zinc catalyst,[12] and 1.34 $A_{C_2H_4}$ cm^{-2} at 68% F.E. for C_2H_4 for a Nafion-coated Cu catalyst.[13]

When an electrocatalyst, subsequently referred to simply as a catalyst, is supported in a GDE, it can be in close proximity to an interface of gas phase CO_2 and a liquid or solid phase electrolyte. Figure 1a shows the cell architecture for a GDE with a supporting aqueous liquid electrolyte and no ionomer binder. Here, it is widely accepted that the high current density in a GDE is enabled by the close proximity of the catalyst and CO_2 gas, allowing for a plentiful supply of CO_2 for the electrochemical reduction. (This architecture will be the focus of this perspective and the assumed architecture for sections 2-5 unless otherwise specified; section 6 will broadly discuss the effects of adding ionomer or using different GDE-cell configurations.)

Looking at the rapidly expanding body of literature using GDE's, however, the nature of where, and how, CO_2 reacts on the electrocatalytic surface in a GDE configuration is not unanimously understood or described. The ultimate question that differentiates the scientific conclusions of many works of CO_2R on GDEs is whether CO_2 reduction occurs at a triple-phase boundary (TPB) or a double-phase boundary (DPB) (see Figure 1).[10,14–30] The meaning of "TPB" is also not unanimous and is oftentimes ambiguous, sometimes with an atomistic context and other times a diffusive mass-transport context. The boundary thickness might be determined in the TPB by the fractions of a nanometer needed to transition from gas to liquid or solid, while in the DPB by the 10s to 1000s of nanometers CO_2 might diffuse through liquid from the gas phase before it chemically or electrochemically reacts.

In the case of the atomistic TPB, CO_2 reduction is described or implied to occur via the direct binding of gas phase CO_2 molecules to the catalyst at gas-liquid-solid junctions. In the case of the atomistic DPB, CO_2 is described to diffuse from the gas-phase to the liquid-phase and be reduced at a liquid-solid DPB in a manner similar to in an H-cell. This latter case is equivalent to the TPB defined in a diffusive mass-transport context, which we will refer to as DPBs within a

triple-phase region. Through the rest of this perspective, we use TPB in the atomistic sense. While the need for a clear phenomenological distinction and common nomenclature may seem inconsequential, the ramifications on catalyst, electrode, and cell design are significant. For example, if the catalyst and support are engineered to maximize atomistic 3-phase interfaces when CO_2R in fact only occurs on the wetted surfaces, then active surface area and reagent transport will be sub-optimal. For this reason, with the rapid rise of literature in this area, we feel that a focused discussion on the nature of CO_2 reduction and its microenvironment near a gas-liquid interface is necessary.

Here, we take a multi-scale approach to clarify the phenomena and nomenclature of the triple-phase region for CO_2 electrolysis on a GDE. **Specifically, this perspective aims to resolve, using well-established scientific theory and observed experimental data, whether an atomistic three-phase or two-phase reaction interface is primarily responsible for the reactivity observed for CO_2R on GDE's.** After first providing a brief history and context for this work, we will assess these two proposed atomistic reaction interfaces from the perspectives of electrochemical and material observations, mass transport of reagents and atomistic reaction pathways, as well as activity and conductivity of the electrolyte. We then provide an overall perspective and outlook for the broader three-phase region which is composed of various interfaces in close proximity to one another, and enables the elevated current densities observed at GDEs. We conclude that water supply to the catalyst is crucial, and the liquid-solid DPB is primarily responsible for the reactivity observed at GDEs, not the atomistic TPB.

2. Background

The first examples of what we term a TPB dates back to H_2 fuel cell work more than a hundred years ago[14], and was repeatedly used later on in the first refined and practical versions of GDEs.[15,16] The reaction rates of gaseous species were proposed to be increased in flow-through and flow-by reactor designs by enabling the contact of the reactant gas with the liquid electrolyte and porous electrodes at the same time. Gas bubbles were pushed through the electrode in flow-through reactors, while a gas stream was passed along the electrode surface in flow-by architectures. Due to the later start and historically slower growth of the electrochemical CO_2 reduction field, many theories and terms were borrowed from fuel cells and batteries. The goal of achieving "a high population of stable three-phase CO_2/catalyst/aqueous electrolyte interfacial sites" was first suggested in the original demonstration of a GDE cell architecture for the CO_2R in 1990.[10] In recent years the same explanation has been used to guide cell design, such as coating Au onto a nanoporous polyethylene hydrophobic film to form "an array of robust and efficient three-phase contact interfaces between gold, H_2O and CO_2 for CO_2R."[17] In another example, Cu powders, dendrites, and wires were supported on both hydrophobic and hydrophilic GDLs to demonstrate whether the hydrophobic support would enhance CO_2R by allowing CO_2 gas "to contact the Cu surface as gas-phase molecules."[18] Numerous other works offer similar explanations for CO_2R activity, many ambiguous on whether the TPB is meant in an atomistic or diffusive mass transport context and which part of the TPB causes the high activity.[19–22]

Other work has recently suggested a TPB is not even present,[23–26] as well as work in 1999 that used a Pt mesh positioned at the interface of CO_2 gas and aqueous electrolyte.[27] They argued "the increase in current at the gas-diffusion electrode is rationalized based on a thin film model. In this model, the pore is considered to be covered by a layer film of electrolyte, which separates

the gas phase from the electrode surface. The gaseous species first dissolves in the outermost layer of the film, and then diffuses to the electrode surface through the electrolyte meniscus. The rate-determining step is the diffusion of gas through the thin layer film, and hence the resulting current should be enhanced as compared with the case of bulk electrolysis in the usual manner."[27] Follow-up work[28,29] was less detailed on this point, arguing that "CO_2 gas is supplied to the electrode surface *directly* from the gas phase." (emphasis added) In light of the conflicting examples above, the confusion and controversy in literature thus may benefit from deeper mechanistic, chemical, and physical understanding to provide clarification.

3. Electrochemical and Material Observations

A first perspective for assessing the dominant reaction interface for CO_2 electrolysis is from electrochemical and material observations of the catalyst layer itself. In short, while a GDL is commonly accepted to be hydrophobic and populated with gaseous CO_2, it is essential to determine from experimental observations whether gas or liquid phases are present in the porous CL. Whether the CL is wetted, partially wetted, or primarily gaseous gives an indication as to the relative availability of three-phase vs two-phase atomistic interfaces within gas-diffusion electrodes.

To begin, we can look at the wettability of flat electrode materials, which describes the preferred affinity of the surface towards water contact or gas contact. While the array of catalysts reported on GDLs is diverse and continuously growing, a substantial percentage of CLs consist of Ag[7,11,23,24] and Cu[7,13,19] deposited onto the MPL of a GDL. We then use these catalysts as a representative case rather than assessing all proposed catalysts. We begin by considering CLs without ionomer.

On an untreated flat metal surface (e.g. metal foil) a water droplet placed on top of these surfaces can exhibit a wide-range of contact angles (Θ, where $\Theta \sim 0°$ and $\Theta > 90°$), indicating that either hydrophilic or hydrophobic surface states are possible.[31] The variability in data is attributed to the presence of different surface-oxide layers,[32] organic contamination, or even contamination from alumina or diamond polishing, all of which can impact wettability. Clean metal surfaces void of these surface layers, however, have been reported to have an effective contact angle of zero ($\Theta \sim 0°$) and are considered to be 'spontaneously-wetted.'[33,34] During CO_2 electrolysis, the reducing potentials are sufficiently more cathodic than those needed to remove most oxide layers, providing a bare metallic surface under ideal conditions. These findings suggest that metal electrodes in an aqueous electrolyte under a reducing potential will exhibit a low contact angle once any non-metallic surface molecules have been removed.

The question now becomes whether rough, porous metal CLs (e.g. spray-coated, sputtered or evaporated metals) with a wide range of thicknesses (from <100 nm to >10 um's) are fully-wetted, or if gas is present within the micro- and nano-pores of a typical CL. In essence, it is necessary to know if gas-liquid interfaces are present only at the boundary of the GDL and CL, or if TPBs are present throughout the entire CL. Here we can use knowledge of the wettability of rough surfaces and capillary action to motivate that the pores of the CL will be wetted if the top layer is hydrophilic under reducing conditions, and there is sufficient electrolyte volume available to fill the porous CL (which may not be the case for zero-gap cells).

Due to the high surface tension of water, a flat material that exhibits hydrophilic contact angles will exhibit increasing hydrophilic contact angles if that same material is roughened, this is termed a Wenzel state.[35] In a Wenzel state, a droplet of water placed on the surface will fill the gas pockets below the top of the rough surface, causing a water droplet to remain physically

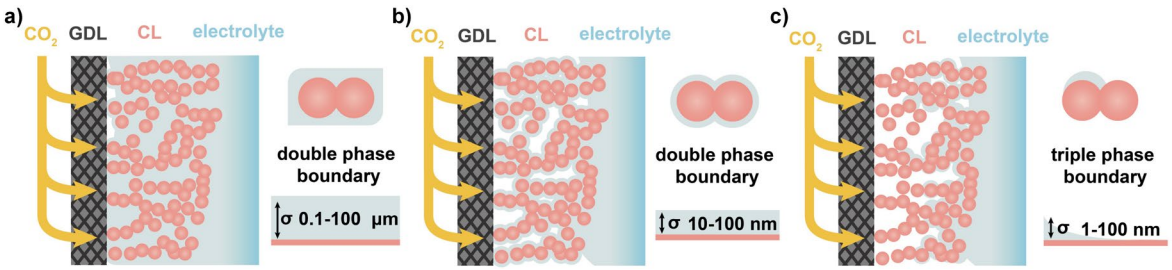

Figure 2. Schematics of possible water arrangements in porous-metal CLs of CO_2R GDEs in contact with an aqueous electrolyte, and magnified images depicting the thickness, σ, of the water layer between gas and catalyst. a) Electrolyte fully flooding the nanopores of the CL, creating a very thick diffusion layer through liquid, with the possibility of TPBs only at the GDL/CL interface. b) An electrolyte film uniformly covering the catalyst particles, with gas in the micropores, containing only DPBs. c) Electrolyte films partially wetting catalyst particles in the nanopores, while gas fills the micropores, creating many TPBs.

'pinned'.[36] For example, Liu et al. showed such pinned droplet states for sputtered Ag and Cu on GDE's both before and after a reducing potential had been applied.[37] Interestingly, Wenzel states for rough metal electrodes are also indirectly confirmed through most CO_2 reduction tests performed in an H-cell. Once water has penetrated the pores of a rough CL in a Wenzel state, the high surface tension will then result in substantial capillary action for micro- and nanopores leading to continued water penetration of the CL (see SI for capillary pressure values vs. pore size).[38,39] Evidence of flooded catalyst pores has also been shown by the residual presence of potassium after electrolysis on a GDE as measured by focused ion beam scanning electron microscopy (FIB-SEM) tomography, though operando measurements could not be made to explicitly conclude this, and the spatial resolution of the energy-dispersive X-ray spectroscopy (EDS) for potassium detection obscured whether only macro-pores flooded, or nano-pores as well.[40]

Water penetration into the porous media will then continue until movement is no longer energetically favorable, which can occur if water approaches a hydrophobic surface (see Young-

Laplace equation). This can occur once the water reaches the GDL (Figure 2a), or if a hydrophobic surface has intentionally been imposed somewhere within the CL (Figure 2c).[41,42] Water penetration can also be counteracted if the external gas pressure is greater than the capillary pressure, as described extensively through models by Ksenzhek and Chizmadzhev.[43] A typical CL, however, has a wide distribution of pore sizes,[40] which through the Young-Laplace equations leads to a wide range of capillary pressures (~291 kPa for a 500 nm pore with $\Theta \sim 0°$) as shown in the SI. Since the CO_2 gas pressure will be constant, a controlled gas-liquid pressure equilibrium throughout the entirety of the CL is then unlikely to be maintained due to variable pore sizes. Increasing gas pressure could then lead to preferential gas breakthrough in the largest pores and cracks in the CL, while the capillary pressure of the smaller pores is more resistant to gas intrusion, as depicted in Figure 2b. To date, the determination of gaseous void fractions has been the most challenging parameter to estimate while modelling GDEs or interpreting experimental data. Although (electro)wetting and mechanical equilibrium inside the pores suggests most of the pores are filled with electrolyte, operando studies are required to determine the (gaseous) void fraction in the CL during operation.

From the above arguments, we can posit that a TPB (gas-liquid-solid) likely exists at the junction of the CL and GDL, while the remainder of the catalytic surface area has a DPB (liquid-solid) if there is sufficient electrolyte available to fill the CL, as depicted in Figure 2a (in our assumed architecture of Figure 1a the volume of electrolyte between the GDE and membrane should be sufficient to fill the CL). Increasing the thickness of a CL would then increase the electrochemically active surface area of the DPB, but not the area of the TPB. If the TPB were primarily responsible for the observed activity of CO_2R, we would then expect little decrease in CO_2R activity as the CL thickness is changed. Unfortunately, no experiments in literature have

specifically been performed to test this hypothesis for CO_2 electrolysis, despite its relative simplicity. In an example of similar experiments,[7] the potential vs. logarithmic current density was compared at different thicknesses of Cu samples (10, 25, 1000 nm sputtered films, and 1000 ug nanoparticle film).[7] As shown in Figure S3, while the slope of $\log_{10}(j_{geo})$ vs. potential of each CL remains similar, suggesting unchanged reaction kinetics, the thicker CLs exhibit lower overall applied potentials for a given current density. This would be expected due to the increase in active surface area. Such behavior indicates that a TPB is not responsible for the majority of the observed current density, as the activity would be relatively similar for all samples.

To test the veracity of this conclusion in a targeted way, we suggest a possible experiment. First, if a simple GDE could be designed with a controlled separation distance between active catalyst and liquid/gas interface, then the separation could be increased from 0 to hundreds of nanometers, and catalyst activity compared. TPBs would be present for the 0 nm separation, but only DPBs for larger separation. If the change in activity was only due to an increased CO_2 diffusion distance through liquid, there would be strong support for DPB reactions providing the majority of reactivity for GDEs.

Finally, in addition to the above argumentation, we note that a typical CL and GDL system is more inhomogeneous than described idealistically above. In reality, an electrode can have multiple gas-liquid interfaces present depending on the deposition technique of a CL onto a GDL and the system configuration. For example, depending on the size of the nanoparticles deposited, or the solvent used, catalytic particles have been observed deep into the GDL.[44,45] Researchers have also intentionally pushed CO_2 through the CL into the liquid phase instead of relying on CO_2 diffusion through the GDL, thus causing a more complicated dynamic system of gas and liquid throughout the various pore sizes of the CL.[22,46] In each of these cases, however, the

reported voltage vs. current data, selectivity, and maximum current density are not substantially different than simpler catalytic systems, even with the likely increase in static or dynamic TPBs throughout the electrode.

Before moving on to a discussion of the transport in these systems, special consideration also needs to be given to CLs deposited with a binding material such as PTFE, or Nafion or Sustainion ionomers. Using a binder is necessary for unique catalytic structures formed via ligand-exchange or wet chemistry approaches to adhere to the support after drop-casting or spray-coating. In such cases the porous CL then consists of more than just a metal catalyst, and could change the water/gas ratio in the pores of a CL, such as those of Figure 2b or c. This may be especially true for PTFE, known to remain hydrophobic under many operational conditions. However, many of the primary reported binders, particularly ionomers, are hygroscopic, and can readily uptake water and swell.[47,48] A bulk ionomer may then exhibit a high water contact angle in a dry-state, but become fully-wetted if water is able to penetrate and expand the polymer matrix.[49,50] The ability for the polymer to uptake water and restructure will however depend upon the composition, structure and functionality of the ionomer.

In conclusion, considering the wettability of the CL suggests that the pores of a metallic CL deposited onto a GDL will be fully-wetted by electrolyte when placed under the reducing potentials needed for CO_2 or CO electrolysis, provided there is sufficient electrolyte present. Under these circumstances, a large fraction of a CL's surface area is then composed of atomistic DPBs (liquid-solid), rather than TPBs (gas-liquid-solid). In the event that CO_2 can access the entire CL by diffusing through the liquid electrolyte, these surfaces are likely to be responsible for the majority of the observed CO_2 reduction activity. While these observations alone do not

exclude the possibility that an atomistic TPB is capable of CO_2R, the discussion here indicates that the primary catalytic activity occurs at a liquid-solid DPB reaction interface.

4. Molecular Perspective on CO_2 Transport Near the TPB

For a better microscopic understanding of CO_2R near TPB and DPBs, we can compare the atomic-scale phenomena occurring at the individual gas-liquid, gas-solid, and liquid-solid interfaces present within a CL. In this analysis, we consider the concentration/activity, diffusion rate, and energetic stability of reactants and products at these various interfaces, which determines the local CO_2R reaction rate. **By comparing the CO_2 activity for TPB and DPB's, we can then assess which region is primarily responsible for the CO_2R reactivity in GDEs.** To navigate this discussion, we follow the diffusion paths available to a CO_2 molecule on its journey from the gaseous GDL towards a catalyst surface, which can be exposed to either a gas or liquid (Figure 3a and b). First, CO_2 diffuses from the flow channel into the GDL until reaching the CL, where it can reach the catalyst surface through several different pathways. In one scenario, the CO_2 molecule can adsorb to the dry catalyst surface (Section 4.1). The CO_2 molecule can then either react with a surface bound hydride or diffuse along the dry catalyst surface to the liquid phase to react with hydride or water (Section 4.2). Here, the binding energy and diffusion rates of CO_2 and hydride on the dry and wet catalyst are assessed to determine the likelihood of these pathways. In a second scenario, the CO_2 can adsorb to the liquid surface, creating a concentrated film of partially-solvated CO_2 molecules,[51] and either diffuse along this film to the catalyst surface, or cross into the liquid phase to diffuse through the liquid electrolyte to the catalyst surface (Section 4.3). The relative diffusion rates and available surface areas or volumes for each of these paths are assessed to determine their relative CO_2 fluxes, and by

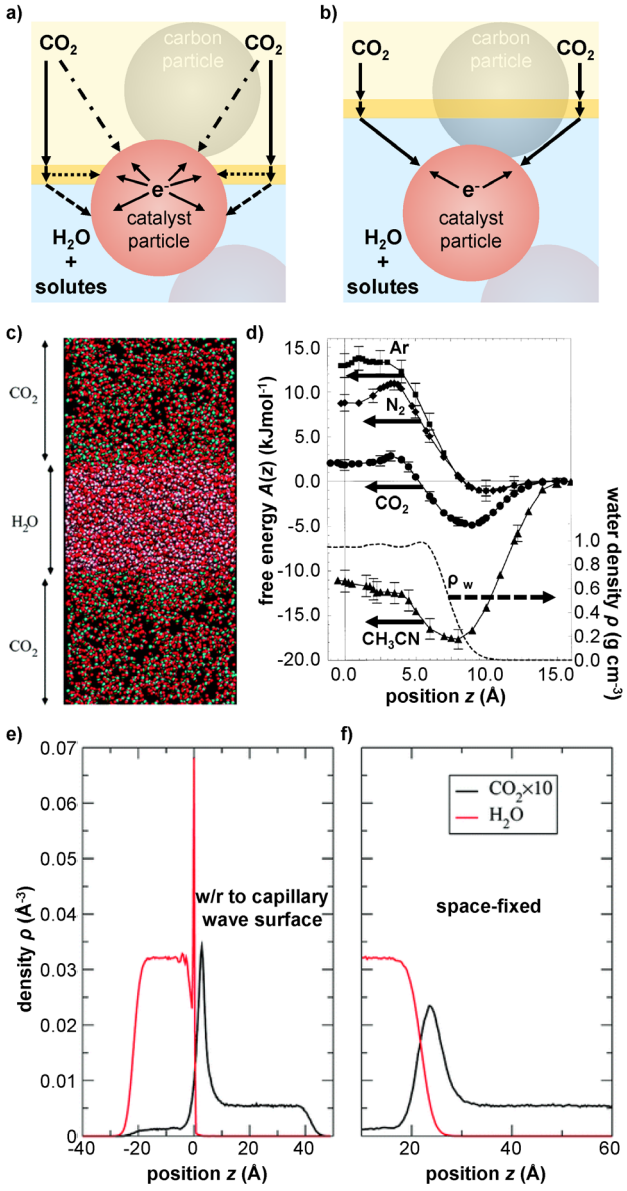

Figure 3. Arrangement of water and gas at the TPB, and the possible CO_2 pathways from gas to the catalyst. a) Schematic of partially wetted catalyst particle, with gas phase CO_2 above and aqueous electrolyte around the sides; dash-dot line shows diffusion directly to gas-solid DPB; long solid line shows CO_2 diffusion through gas to liquid surface, dotted line shows CO_2 diffusion along gas-liquid DPB, short solid line shows diffusion across gas-liquid DPB, dashed line shows diffusion through liquid. b) Schematic of a fully wetted catalyst particle, with a film of water between the gas phase CO_2 and the catalyst surface; solid arrows show the approximate CO_2 diffusion path (for full wetting of catalyst particle, adjacent carbon particle of GDL likely becomes partially wetted). In (a,b), faded carbon and catalyst particles are shown adjacent to catalyst particle of focus for context. c) Cross-section of water slab and CO_2 gas. d) (left axis) The free energy barrier for CO_2 and N_2 to enter electrolyte, (right axis) the

density of water. e) Density profile of water (red line) and CO_2 (black line) with respect to the "capillary wave surface" of the water; f) with respect to a space-fixed coordinate system. Panels c,e,f reproduced and modified with permission from [52]. Copyright 2011 American Chemical Society. Panel d reproduced and modified with permission from [51]. Copyright 1999 Royal Society of Chemistry.

extension the CO_2 activity. Assumptions that the catalyst is surrounded by pure water are made when relevant data and simulations for common electrolytes are unavailable in the literature.

4.1 CO_2 binding to dry solid surface

Once the GDL is filled with gaseous CO_2, we first consider the possibility of a CO_2 molecule binding to a dry catalyst under conditions relevant for CO_2R (dash-dot path in Figure 3a). Adhesion of CO_2 to a dry electrocatalyst's surface, and subsequent diffusion of CO_2 along this surface, determines the extent to which the dry surface may act as a reactant feed to the wetted catalyst surface and contribute current density to the net GDE current. In essence, we are trying to determine if a dry electrocatalyst surface can be favorable to have in a CO_2R system. We again use Cu and Ag as central examples due to their affinity for high CO_2R activity in GDEs.

Our original intuition was that such adhesion wouldn't be possible. This was guided by early work[53–57] performed under ultra-high vacuum (UHV) conditions, which found that CO_2 can physisorb directly to Cu and Ag only under low temperatures. Upon warming of the surface, the CO_2 desorbs from Cu at different temperatures depending on the surface facets (21 K (Cu (110)),[55] 130 K (Cu (211)),[54,56,57] and between 80 and 295 K (polycrystalline Cu)).[54] For a clean Ag(111) surface, the CO_2 desorbs above 40 K.[53] Surfaces contaminated by oxygen, however, bound the CO_2 until somewhat higher temperatures, such as 130 K on a Ag(110) surface with

oxygen adatoms.[53] Unfortunately, physisorbed CO_2 is a linear molecule and not useful for CO_2R, which requires bent chemisorbed CO_2 (b-CO_2).[58]

More recently, CO_2 adsorption to Cu(111) was studied by ambient pressure X-ray photoelectron spectroscopy (APXPS) measurements and supporting density functional theory (DFT) calculations.[59] Here, b-CO_2 was observed at 298 K under 0.7 Torr, much closer to CO_2R standard operating conditions than the UHV experiments. Since DFT calculations indicated 33 atm would be necessary for CO_2 to bind to pristine Cu at 298 K, it was hypothesized that b-CO_2 was stabilized on the surface by suboxide layers and the addition of water vapor.

A similar study on Ag found CO_2 binding to both pristine and oxygen coated surfaces, with binding occurring faster in the latter case (Figure S4a).[58] Here the presence of water stabilized b-CO_2 on the Ag in two configurations. DFT calculations predicted one of these to mediate CO_2R via the same intermediates as Cu, while the other to mediate CO_2R via a more facile path.

Actual CO_2R conditions include a reducing potential on the catalyst surface, which could reduce the metal oxide and prevent the O layer from being present during electrolysis. Only operando measurements can then provide an authoritative assessment of the presence of O on the Cu or Ag surface during CO_2R, since oxidation of the surface could occur as soon as the reducing electric potential is turned off. We are aware of two such operando measurements during CO_2R, one showing continued presence of O on a Ag catalyst[60] and the other showing its absence.[61] Thus, to answer our initial question, catalytically reactive b-CO_2 adsorption to dry Cu or Ag appears to be possible, and faster in the presence of water vapor.

4.2 Transport of CO_2 along a dry and wetted catalyst surface

Once a CO_2 molecule becomes physisorbed or chemisorbed to a dry electrocatalyst surface, **there is the question of whether this adsorption contributes measurably to CO_2R**. In the case where CO_2 adsorbs in close proximity to an atomistic TPB, there are two conceivable pathways for the bound CO_2 molecule to be electrochemically reduced: (1) diffusion of CO_2 along the dry catalyst surface into the liquid electrolyte phase where it is reduced at the liquid-solid DPB; or (2) diffusion of an adsorbed hydride ion from the liquid phase into the gas phase, where it would react with CO_2 adsorbed at the gas-solid DPB. The expected contribution to CO_2R, in either case, is then dependent on the relative rate of surface diffusion of CO_2 and hydride ions along dry and wetted catalyst surfaces as compared to other diffusion mechanisms (CO_2 diffusion directly into the liquid phase).

Considering the first case, we can compare the diffusive flux of CO_2 along the catalyst surface to the diffusion flux of CO_2 through the liquid phase to determine their relative rates, for a stagnant capillary height in the porous electrode. Using Arrhenius kinetics to describe the surface diffusion, the energy barrier to surface diffusion can be estimated from the desorption activation energy through a corrugation ratio, explicitly the ratio of diffusion activation energy to desorption activation energy, which typically ranges from 0.25 to 0.30 for gaseous adsorbates on metal surfaces. Assuming a corrugation ratio[62] of 0.25 and a desorption activation energy for CO_2 on Ag[63] of 84 kJ $mole^{-1}$ yields a surface diffusion coefficient of $3*10^{-8}$ cm^2 s^{-1} at room temperature. This is characteristic of a weakly chemisorbed system[64] and three orders of magnitude less than the diffusion coefficient of CO_2 in water ($2*10^{-5}$ cm^2 s^{-1}).[65] Calculations in the SI, which account for the differences between surface and bulk diffusion, found that the relative flux of CO_2 along the catalyst surface is more than an order of magnitude smaller than

the flux of CO_2 diffusing through the gas-liquid DPB (assuming a circular 50 nm diameter CL pore). Thus, based on the larger mass transfer rate for CO_2 diffusion directly through the gas-liquid DPB, it is unlikely that surface diffusion of CO_2 along the dry catalyst plays a relevant role in the observed high current densities during CO_2R on a GDE.

For the second case, we consider the rate that a hydride ion can diffuse from the liquid to the gas phase to react with CO_2. To determine the maximum CO_2R current possible from this reaction route, calculations were performed using data for hydride surface diffusion on a Cu(100) surface at a gas-solid DPB.[66–68] These results showed even if hydride surface coverage dropped to zero within 0.5 nm of the atomistic TPB, surface diffusion cannot compensate for measured CO_2R activities. For a pore of diameter 50 nm, the limiting geometric mass transfer due to surface diffusion was $2.5*10^{-17}$ mol s^{-1} of hydride out of one pore. Normalizing this rate to the 50 x 50 nm square that encompassed the pore yielded a geometric flux of $2.5*10^{-7}$ mol cm^{-2} s^{-1}, equivalent to a maximum geometric CO_2R current density of 24 mA cm^{-2}. The calculated limiting current density due to surface diffusion of hydrides is less than measured geometric current densities on porous Cu electrodes with similar pore sizes,[7] and therefore hydride surface diffusion is likely not the main mechanism through which the reaction proceeds at high current densities. The rapid replenishment of surface hydrides at the TPB would require very high water activity close to the TPB, which is unlikely based on the discussion in section 5.1.

In summary, by examining both viable reaction routes originating from the direct binding of CO_2 to a dry catalyst surface, we conclude that the majority of CO_2R activity must occur from CO_2 reaching the catalyst's surface via the liquid phase, and not the gas phase.

4.3 CO_2 transport along liquid surface or through liquid bulk

Finally, a transport mechanism that is relevant to the phenomena occurring at a TPB is the movement of CO_2 into the liquid phase (paths beginning with long solid line in Figure 3a). The phenomena relevant for predicting possible electrochemical activity include (i) the physical properties of the CO_2-liquid film, (ii) the transport of CO_2 through the film, and (iii) the transport of CO_2 along the film.

Using known energetics of CO_2 molecules near the liquid surface, density functional theory (DFT)[51,52] and molecular dynamics (MD) simulations[69] can describe the CO_2-water interaction. These simulations show a result not discussed in CO_2R literature, that a CO_2 film is present at the gas-liquid DPB.

These models typically use a horizontal slab of water with CO_2 gas above and below, as depicted in the 3D illustration of Figure 3c.[52] The calculated free energy of CO_2 showed an energy minima of ~5 kJ/mol, twice the energy of thermal motion for the 300 K system, and sufficient to form the film of CO_2 molecules on the gas-liquid DPB. The calculated density of CO_2 and water are plotted in Figure 3e-f, with each panel using a different mathematical definition for the water surface, showing the water surface transitions from 0 to bulk water density in ~0.2-1 nm and CO_2 adsorbs to the water surface in a ~1 nm thick film. The film has 5-7x the density of CO_2 in the gas phase, and 16-25x the density of CO_2 dissolved in the liquid water. Other common gasses show a similar energy profile, but with different magnitudes of energy wells and barriers; this suggests gas products from CO_2R may experience different kinetics at the gas-liquid DPB than CO_2.

It is useful to now consider CO_2 diffusion through the liquid layer to the catalyst surface (short solid line and dashed line in Figure 3a). The flux of CO_2 along this path will depend on the rate

of diffusion across the gas-liquid DPB, the rate of diffusion through liquid, the area of the wet catalyst, and the concentration of CO_2 in the liquid. These diffusion rates have been determined by MD simulations and validated against experiments (see SI for detailed summary).[69] The first question to address is how far into the liquid a gaseous CO_2 molecule can penetrate before it acts like a dissolved CO_2 molecule. MD simulations found that CO_2 molecules thermalize rapidly at the liquid surface, losing their gas-phase kinetic energy in 0.3±0.05 ps, per the simulated decay in average kinetic energy shown in Figure S4c. This thermalization occurred mostly within ~0.5 nm, where the liquid density went from 0 to bulk, per the histogram of velocity reversals of a CO_2 molecule as a function of position in Figure S4d. This rules out any possibility of CO_2 molecules passing through a layer of liquid to reach the wetted catalyst surface before becoming solvated in the liquid, unless the water layer was only several monolayers thick (i.e., <0.5 nm).

Next, it is necessary to understand whether the process of crossing from gas into liquid phase is faster or slower than CO_2 diffusion through the liquid phase. Previous results indicate that this transition between phases is faster,[69] despite the small energy barrier between the CO_2 film and inside the liquid phase (Figure 3d). Thus, in the path in Figure 3a for CO_2 diffusing from gas to the liquid-solid DPB, the dashed line is the slowest path portion.

Lastly, we consider the possible flux of CO_2 along the CO_2 film (dotted line in Figure 3a). It is apparent in Figure 3e that the high concentration of CO_2 corresponding to the CO_2 film is positioned where the water density is below 50%. If we approximate D by the relation for a 2-dimensional gas,

$$D = \frac{1}{8nd}\sqrt{\frac{2\,k_B T}{m}}, \qquad \text{Eq. 1}$$

where n is the number density of molecules, d the molecule diameter, k_B the Boltzman constant, T absolute temperature, and m the molecule mass, then we can see that D scales inversely with

density. Thus, a 50% to 90% decrease in water density should increase the diffusion rate by 2 to 10x. This compounds with the 16 to 25x increase in CO_2 concentration in the film compared to that dissolved in liquid, per Figure 3e-f. Combined, these rough values suggest a ~30 to 250x increase in flux per unit area along the CO_2 film compared to the flux in the liquid. On the other hand, the CO_2 film is only ~0.5 nm thick, while the wetted catalyst surface could be anywhere from 10 to over 10,000 nm thick.[40]

In short, this subsection discussed the transport of CO_2 from the gas phase to the liquid phase, which is highly relevant for the discussion of CO_2 electrolysis on GDEs. While a concentrated CO_2 film on the liquid may be a beneficial place to position a catalytic surface due to higher CO_2 concentrations and faster transport than a bulk liquid phase, the cross-sectional area of such a film is relatively small. Thus, the catalytic surface with access to such a film is likely much smaller than the area of the liquid-solid DPB as described in Section 3.

In conclusion, this section has discussed the various transport mechanisms for CO_2 occurring near the gas-liquid interface. While the diffusion rate of CO_2 through the gas phase is faster than any other phase, the diffusion of $CO_2^{\cdot-}$ and hydride along the catalyst surface is slow relative to other transport mechanisms. While the CO_2 film concentration and diffusion rate are high, it's contact area with the catalyst is much smaller than the liquid-solid DPB. In both cases, larger geometric current densities are possible with smaller pores, however, this process would be limited by water activity at the atomistic TPB, as described in the subsequent section. Thus, this section suggests the liquid-solid DPB is primarily responsible for the activity in a CO_2R GDE and not the TPB.

5. Current Distribution in Wet Catalyst Layers

In the previous section, the transport and binding of CO_2 at various interfaces in a CO_2 electrolyzer were discussed, using the fluxes of a CO_2 molecule to infer activity (Figure 1b). Here, the local reaction rate that is possible at the wet catalyst surface is discussed, which may be within a flooded CL (Figure 2a) or may have a thin electrolyte film coating it (Figure 2b or 2c). At this wet catalyst surface, the reaction may be limited by the water activity and the ionic conductivity rather than access to CO_2. Furthermore, the water activity and electrolyte concentration may control CO_2 transport by affecting its solubility, diffusion, and conversion to (bi)carbonate. When combined with the discussions so far, and using focused literature from the hydrogen oxidation reaction (HOR) and oxygen reduction reaction (ORR) literature as guides, the limitations of electrochemical reactions in thin electrolyte films is discussed below to better understand the length scales important for each parameter affecting electrochemical CO_2R.

5.1 Effect of water activity on reaction rate and CO_2 supply

At the same rate that electrons are transferred to a CO_2 molecule during CO_2 electrolysis, a source of protons is also required. In aqueous electrolytes, water plays a critical role by providing protons to the reaction, but the availability of water in an electrolyte (called the water activity) is finite and may be limited under certain conditions, particularly at elevated electrolyte concentrations and thin film thicknesses.

The water activity represents the ability of water molecules to hydrate ions in solution. It is defined to have a value of 1 for pure water and drop toward zero with increasing solute concentration.[70,71]

For neutral pH solutions containing a buffer electrolyte (e.g. 0.5 M $NaHCO_3$, pH 7.2) the protons are shown to be supplied by the buffer anions at low overpotentials on Cu electrodes, which results in mass transfer limited current density depending on the convective forces and electrolyte concentration.[72,73] Recent work on Ag electrodes[74] has suggested the first protonation of CO_2 is from HCO_3^-, and the second pronation from H_2O, with the second protonation the rate-determining step (RDS) for nanostructured Ag electrodes, as shown in Eq. 3. This corresponds to a reaction of order -1 in CO_3^{2-} and of order 1 in P_{CO_2}, HCO_3^-, and H_2O. The overall chemical reaction is then,

$$\mathrm{CO_2 + HCO_3^- + H_2O + 2e^- \rightarrow CO + OH^- + CO_3^{2-} + H_2O} \qquad \text{Eq. 2}$$

Broken down into sequential steps, this is

$$\mathrm{CO_2 + HCO_3^- + e^- + * \rightarrow COOH_{ads} + CO_3^{2-}} \qquad \text{Eq. 3.1}$$

$$\mathrm{COOH_{ads} + H_2O \xrightarrow[RDS]{} COOH_{ads}\ldots H^+ + OH^-} \qquad \text{Eq. 3.2}$$

$$\mathrm{COOH_{ads}\ldots H^+ + e^- \rightarrow CO_{ads} + H_2O} \qquad \text{Eq. 3.3}$$

$$\mathrm{CO_{ads} \rightarrow CO + *} \qquad \text{Eq. 3.4}$$

The corresponding rate expression for CO_2R to CO is then,

$$i_{\mathrm{CO_2R}} = -nFAk^0 \frac{a_{\mathrm{CO_2}} a_{\mathrm{H_2O}} a_{HCO_3^{2-}}}{a_{CO_3^{2-}}} e^{-\alpha_c f \eta},$$

where n is the number of electrons per CO_2 molecule, F the Faraday constant, A electrode area, $f=F/RT$, with R the gas constant and T absolute temperature, α_c is the cathodic charge transfer coefficient, and η is the overpotential. Note that this and alternative RDSs, along with the order of dependence in bicarbonate, were proposed at low potentials since at high potentials mass transport effects were assumed to effect the Tafel slope.[75]

More importantly, at high potentials the protons are considered to be supplied by water molecules as the proton reduction (either from solvated protons or from the buffer electrolyte) reaches to a mass transfer limitation.[72] Therefore, for GDEs most of the protons are likely to be supplied by water molecules at high current densities. Further, due to electrostatic repulsion, the proton donated to a CO_2R intermediate already bound to the negatively charged cathode is expected to come from the neutral H_2O molecule rather than the negative HCO_3^-; thus, many possible rate expressions will include water activity, and water activity will likely be an important factor in the CO_2R rate expression for GDEs.

To confirm these for GDEs operating in neutral or alkaline electrolytes (e.g. KOH), further work will be necessary. Specifically, the operando activity of solutes and the solvent in the microenvironment of the GDE must be measured to determine the reaction rate dependence on solute activity, and this data coupled with Tafel analysis to evaluate possible RDSs.

The above equation shows a linear dependence of current on water activity, $i_{CO_2R} \sim a_{H_2O}$, (first order reaction in H_2O) which would preclude significant reaction rates at low water activity. This dependence could affect the current distribution in a CL in two ways. First, water films of ~3 nm or less have been predicted to have low water activity.[76] Second, the accumulation of OH^- from CO_2R (and consequent accumulation of cations, e.g. Na^+ or K^+) in a pore of the CL far from the bulk electrolyte will result in a high local electrolyte concentration,[25] and thereby a low local water activity and CO_2R reaction rate.

To determine which part of a GDE CL is primarily responsible for the CO_2R activity, it is apparent that local water activity in the CL microenvironment will favor higher reaction rates closer to the electrolyte bulk (further from the gas-liquid DPB), because there will be less electrolyte ion accumulation and higher water activity.

5.2 Electrolyte conductivity

The electrolyte conductivity also has an important effect on the distribution of j_{CO_2R} in the CL. The CO_2R reaction, as with the HOR and ORR, is an electrochemical reaction that requires ions traveling to and from the reaction site in order to complete an electrical circuit. Unlike the electrically neutral CO_2 molecule, which when near the electrode can only undergo diffusion, charged ions like OH^- can be transported by diffusion as well as migration, the latter driven by an electric field. This migration causes a drop in voltage across the electrolyte that is proportional to its ionic resistance, as described by Ohm's law.

Several conditions could cause low electrolyte conductivity in a CL. Near the tip of an electrolyte meniscus, such a meniscus being found at the TPB of a porous electrode, the electrolyte layer becomes thin and the ionic resistance increases.[77] The ionic resistance in porous electrodes is also greater at points in the electrode further from the electrolyte bulk, due to the long narrow channels of electrolyte that ions must travel through. Partial flooding of porous electrodes means some channels through the electrode will be filled by gas rather than electrolyte, and such channels will have no ionic conductivity, thereby increasing the net ionic resistance of the CL.[43] Finally, the local increase in electrolyte concentration in the CL from production of OH^- should increase electrolyte conductivity until 5 M for NaOH, or 7 M for KOH, (25 °C) after which the conductivity will decrease.[78] The high electrolyte conductivity has been suggested as the reason CO_2R at GDEs in 7 M KOH showed low overpotentials for high current densities of approximately 1 A cm^{-2} (although CO_2 consumption by concentrated KOH presents energy efficiency challenges).[13,19,79]

The importance of electrolyte conductivity has recently been experimentally demonstrated for CO_2R on GDEs at high current densities (>100 mA cm^{-2}), although this study only varied the bulk conductivity.[80]

5.3 Estimated size of reaction zone

From the above assessment of mass transport and reaction rates at different phases and phase boundaries, we can assess the physical size of the catalyst area that contributes to the majority of the reactivity/current in a GDE, and understand how close it typically is to the gas-liquid DPB. Looking first to the mature field of fuel cells for precedents, we consider a study of the HOR that measured the meniscus shape on a vertical flat Pt electrode partially immersed in 1 N H_2SO_4.[76] The meniscus had a finite contact angle (~3º) at its tip (Figure S5a) and extended down approximately 500 μm to where the electrolyte surface became horizontal (Figure S5b). Calculations of the current distribution along the Pt surface found that at 0.91 V vs. RHE, 50% of the current was within the first 1 μm of the meniscus tip, and at 0.39 V vs. RHE, 50% of the current was within 6 μm of it (Figure S5c and d). Thus, the calculated current distribution extended 1000s of nm from the meniscus tip, beneath an electrolyte film ranging from 3 to ~300 nm thick.

Next, we consider modelling of a CO_2R GDE with a porous Ag CL devoid of ionomer (an inert binder was assumed). The GDE architecture is shown in Figure 4a. For the case of a CL fully flooded by the electrolyte, Figures 4b and 4c show the depth dependence of j_{CO} and CO_2 concentration in the CL (depth scaled by the CL thickness of ~4 μm, per calculation in the SI). Low current densities see an even distribution of CO_2 and j_{CO} throughout the CL. High current densities see depletion of CO_2 in the CL, with confinement of dissolved CO_2 and j_{CO} to the CL

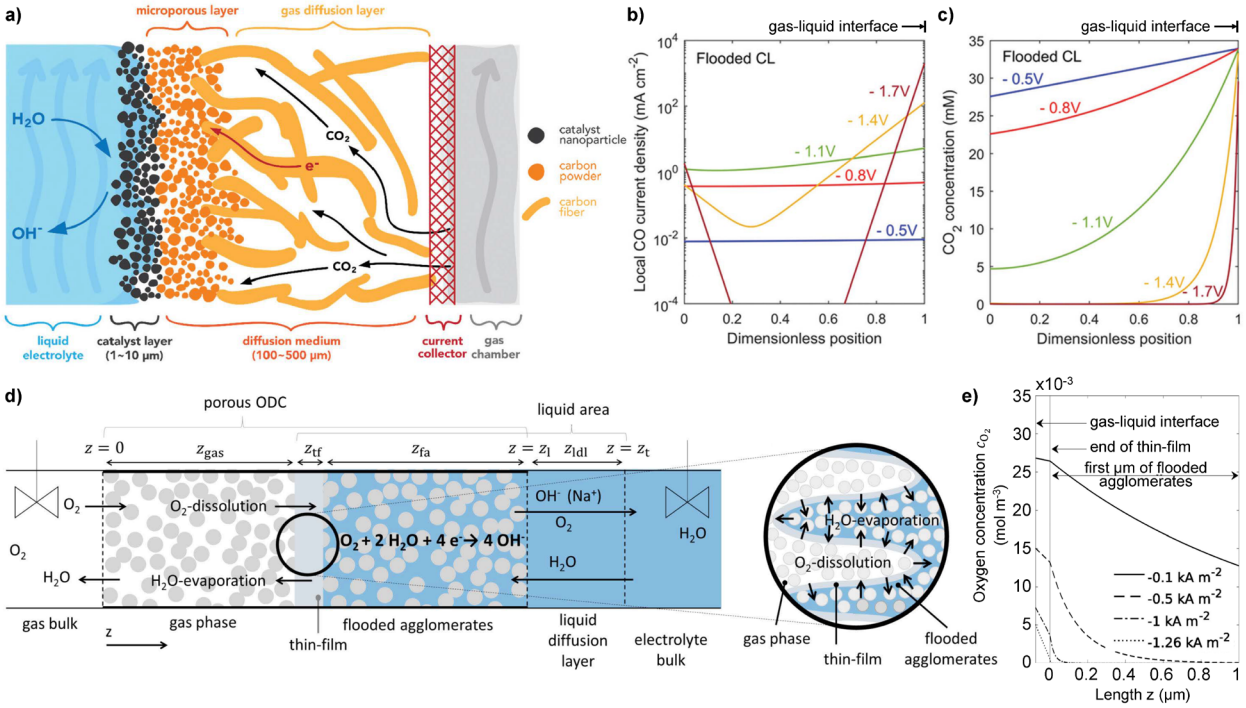

Figure 4. Detailed study of CO_2 and O_2 diffusion in CO_2R and ORR GDEs, with comparison between experiment and simulation. a) Diagram of the CO_2R GDE. b) Simulated CO_2R to CO current density, j_{CO}, profile vs. depth into CL. c) Simulated CO_2 concentration profile vs. depth into CL. b-c) Depth dimensionless position scaled by CL thickness of ~4 μm. d) Diagram of partially flooded CL in the ORR GDE. e) Simulated O_2 concentration profile for different current densities, in the case of no stirring in the electrolyte bulk. Panels a-c reproduced and modified with permission from [25]. Copyright conveyed through Copyright Clearance Center, Inc. Panels d,e reproduced and modified with permission from [81]. Copyright 2019 Creative Commons License.

portion near the gas-liquid DPB; the highest j_{CO} shows a drop in j_{CO} of 2 orders of magnitude within ~200 nm from the gas-liquid DPB. This model did not include parameters like water activity or variable water concentration. However, it found the electrolyte concentration could surpass 10 M KOH in the CL despite a bulk electrolyte of 0.5 M $KHCO_3$; the authors suggested it would behoove future work to include such parameters.

For insight on the role of water activity on current distribution, we can look to a study of the ORR in the CL of a fuel cell cathode. This study also demonstrates techniques for careful validation of simulations against experiment. The GDE architecture investigated is shown in Figure 4d.[81] In the model, the gas-liquid DPB between dry and flooded agglomerates was contained in the so-called "thin-film" region, assumed to be 80 nm thick, and the reaction zone, where the ORR occurred, was confined to the flooded agglomerate region. Figure 4e shows the simulated O_2 concentration profile throughout the thin-film and flooded agglomerate regions for four values of j_{ORR}, in the case of a stagnant (unstirred) electrolyte bulk. The reaction zone, defined by the O_2 profile, shrunk "almost to zero at the mass transport governed current density of j_{ORR} = -1.26 kA m^{-2} " (-126 mA cm^{-2}). However, stirring the electrolyte bulk lowered the accumulation of OH^- and Na^+ in the flooded agglomerate, maintaining high water activity for high O_2 solubility, and low viscosity for fast O_2 diffusion, preventing the reaction zone from shrinking to zero.

Using the dissolved O_2 concentration profile as a first order approximation for the j_{ORR} profile, the reactive area of the CL seems to extend 10s to 1000s of nm from the gas-liquid DPB, depending on the current density. Convolution between the dissolved O_2 concentration profile, electrolyte conductivity, and water activity should shift the region of highest j_{ORR} deeper into the flooded agglomerates, further from the O_2 gas. Crucially, by including water activity they demonstrated it dictated the O_2 concentration profile and thereby the j_{ORR} profile.

To summarize, relevant models support the assumption that the reaction zone for CO_2R in a GDE is confined to the wet portion of the CL, and suggest the j_{CO} distribution in a fully flooded CL is determined largely by the dissolved CO_2 distribution. Further, this reactant gas distribution is apparently regulated by the electrolyte concentration at high current densities (~100 mA cm^{-2}).

In the CO_2 case, the CO_2 equilibrium with (bi)carbonate plays an important role, with high local hydroxide concentrations consuming CO_2, which will limit CO_2 penetration into the CL.[25,82,83] Also, as demonstrated for the ORR,[81] the high electrolyte concentration in the CL will increase viscosity, thereby slowing diffusion of CO_2 and diminishing electrolyte conductivity.[78] Thus, the portion of the CL primarily responsible for the CO_2R current likely extends 10-1000 nm from the gas-liquid interface, with a thinner reaction zone at higher current densities, and a current distribution as depicted in Figure 1b.

6. Assessment and Outlook

The above considerations are focused on porous metal CLs devoid of ionomer and supported on GDLs to form GDEs for electrochemical CO_2R. From the physics of wetting porous materials, it was established there is a strong propensity of nanopores and micropores in the CL to be flooded by an aqueous electrolyte, such that most reported CLs can be assumed to be fully flooded. From reported increases in GDE activity with increased CL thickness (Figure S3), it was established the electrochemical response of GDEs can be explained by a model where CO_2 diffuses from gas phase, through liquid, to reach the catalyst. Together, these materials and electrochemical observations suggest the **atomistic liquid-solid two-phase reaction interface is primarily responsible for the reactivity observed for CO_2R on GDE's and not the atomistic triple-phase boundary where most researchers claim.**

Probing the question from another perspective, molecular mass transport and thermodynamic stability were used to explain how a reaction could happen in different parts of an atomistic TPB. At the dry catalyst surface, a gas-phase CO_2 molecule can chemisorb to the surface in a manner amenable to CO_2R, given the likely presence of water vapor in close proximity to the TPB.

However, calculations of the approximate diffusion rate of bound CO_2 or hydride on the metal surface suggested the reaction zone would be limited to ~1 nm from the TPB, and that diffusion rates would be slower than CO_2 dissolving into the water and then to the catalyst surface.

At the DPB of CO_2 gas and liquid water there is a concentrated film of CO_2 at the water surface, which is calculated by DFT to be about 1 nm thick, with a CO_2 diffusion constant between that of the gas and liquid phases. While this implies a greater per-unit-surface-area supply of CO_2 to the TPB than the wet catalyst surface, the reaction zone will be only 1 nm thick, while the wet catalyst surface extends 10s-1000s of nanometers depending on the CL composition and the total current density.

Due to the dependency on protons for CO_2R, CO_2 supply is only half the story for determining the CO_2R reaction rate. In alkaline electrolytes, H_2O is consumed and OH^- produced by CO_2R. Thus, the low water activity in thin water films and concentrated electrolytes should slow the reaction at the thin electrolyte layer of a meniscus, or deep in a porous electrode (far from bulk electrolyte) where OH^-, and therefore cations such as K^+, accumulate in high concentrations such as 10 M KOH.[25] This high local electrolyte concentration should also lower the CO_2 solubility and diffusion rate, and lowers local ionic conductivity in highly concentrated electrolytes (above 7 M for KOH). Furthermore, thin water films, partially wetted CL pores, and pores far from the electrolyte bulk have low ionic conductivity, causing ohmic resistance to OH^- migration from the reaction zone. Thus, these two parameters, water activity and electrolyte conductivity, favor a higher reaction rate near the electrolyte bulk, away from the TPB. Combining the limitations of CO_2 supply, H_2O supply, and OH^- migration, **we expect CO_2R current to be primarily at the catalyst surface in the liquid phase, with a reaction zone extending 10s-1000s nm from the**

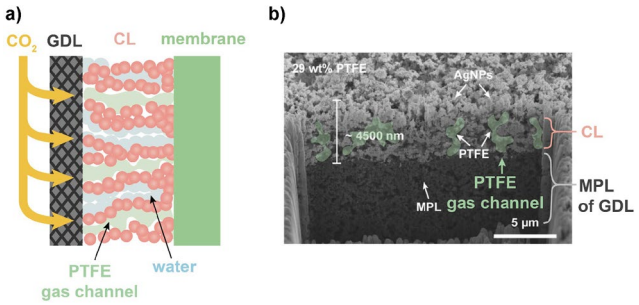

Figure 5. Zero-gap GDE cathode. a) Schematic of expected water and CO_2 distribution in the CL. b) SEM image of cross-section of CL, showing segregated regions of Ag catalyst and PTFE; annotations show the expected gas channels in the PTFE regions. Panel b) reproduced and modified with permission from [8]. Copyright 2020 American Chemical Society.

gas phase, a similar size to that of the HOR and ORR systems discussed, with a current distribution approximately as shown in Figure 1b.

The utility of the above conclusions is in understanding different GDE cells' performance and pathways to improvement. As already discussed, for GDE cells that rely on liquid water infiltration of the CL to supply water and ionic conductivity to the catalyst, cells fall into three categories: microfluidic cells with flowing electrolyte and no membrane, hybrid cells with a gap for liquid flow between the GDE and membrane, and zero-gap cells with the GDE pressed directly against the membrane. For all three architectures, the water distribution in the CL is a function of pore size, (hydrophobic) PTFE content, and availability of water for pore filling. Given the expected physics of pore flooding, a nanoporous metal CL in contact with a liquid electrolyte would have a fully flooded CL and fully dry GDL, as depicted in Figure 2a. If the pores were large enough, then it is possible the catalyst surface may fully wet without flooding the pores, to create a CL as depicted in Figure 2b. Finally, if PTFE was included in the CL (as it sometimes is for binding together catalyst particles or managing CL flooding), it could create dry regions, and look like the CL as depicted in Figure 2c. This last water arrangement is especially

likely for zero-gap cells, since the water for filling the CL is constrained to condensation from a humidified gas stream and water diffusion through the membrane. High loading of PTFE in a CL made of carbon particles, PTFE, and Ag particles has shown the Ag and PTFE to segregate into ~1 μm regions,[8] and in zero-gap cells these regions may mediate adjacent flooded catalyst-filled regions and dry PTFE regions, as depicted in Figure 5.

The CO_2R current distribution in the CL can be surmised from the above summary of CL flooding and the results of Section 5 on the wet CL current distribution in triple-phase regions. In a fully flooded CL, on a fully dry GDL, sufficiently low current densities would render 1000s of nanometers of CL thickness active towards CO_2R, while sufficiently high current densities would likely confine the activity to the first 10-100 nm from the gas phase (because CO_2 diffusing through the liquid would be consumed by the first 10-100 nm of catalyst due to the high reaction rate). For zero-gap cells, partial flooding of the CL could explain the sensitivity of these cells to process conditions. Insufficient flooding of the CL may cause low water supply and low ionic conductivity to the catalyst, while excessive flooding may reduce the CO_2 supply to the wet catalyst regions. Optimum CO_2R may be achieved from flooded ~1 μm wide channels of catalyst filled regions with interdigitating ~1 μm wide channels of dry PTFE filled regions. Since ionomers, also often used as a catalyst binder, conduct water and ions, their inclusion in the flooded channels of the CL in Figure 5 may benefit GDE performance, although we are not aware of any studies on this combination of PTFE and ionomer. These ionomer binders, such as Nafion, also support CO_2 diffusion[84] and have enabled some of the best-performing CO_2R GDEs.[13]

For both liquid electrolyte and zero-gap cells, flooding of the GDL is likely to diminish CO_2 supply to the CL with no benefit to water activity or electrolyte conductivity. This GDL flooding

is a widely reported issue in GDE cells,[8,17,45] but unfortunately there are no definitive studies that can distinguish how much flooding occurs in the CL vs. the GDL. Operando tomography, demonstrated in adjacent research fields on Ag GDEs[85] and polymer electrolyte fuel cells,[86] could provide useful insight into CO_2R GDEs.

Going forward, the apparent advantage of a TPB near the catalyst is providing a short diffusion path for the gas, through liquid, to the catalyst. As higher current densities are reached, and GDEs are devised that provide significant catalyst surface area near the CO_2 gas, water management to ensure a plentiful water supply will likely become increasingly important. Likewise, any such electrodes will require high ionic conductivity with the current well-distributed over the surface to avoid high localized current densities with corresponding high ohmic drops. Finally, creating stable gas channels and liquid channels in the CL of a zero-gap cell may provide an optimal supply of CO_2, H_2O, and ion conductivity to the catalyst, although ensuring the catalyst was in the liquid phase would be necessary to maximize its utilization.

Conclusions

To conclude, there is uncertainty in the literature of CO_2R on the role of the TPB in GDEs. We have considered wetting properties of GDEs to suggest what the likely water distribution within them is, and electrochemical observations of CO_2R GDEs that support a picture of CO_2 diffusing a short distance from gas, through liquid, to the catalyst. Further, we considered molecular scale mass transport and energetics of reactants and products in the different phases and their boundaries, which supported a picture where CO_2R occurs primarily in the liquid covered catalyst. This result is similar to the conventional models for the spatial current distribution for HOR and ORR electrodes used in fuel cells, a more mature and well-studied technology than

CO_2R. These electrochemical systems were chosen as parallels to CO_2R because they consume reactant gases, and ORR in particular consumes water and produces OH^-, similar to CO_2R. These systems showed the reaction to occur primarily within 10-1000 nm of the gas-liquid interface. At higher current densities, the current was confined closer to that interface.

From our analysis, CO_2R should be regulated by the water activity and electrolyte concentration similarly to the HOR and ORR. Thus, the above results suggest that, in going forward to higher current density CO_2R reactors, there should be a focus on both CO_2 diffusion to the catalyst, as well as maintaining a moderate electrolyte concentration that has slow CO_2 conversion to (bi)carbonate with high water activity and ionic conductivity in the microenvironment of the catalyst surface. Finally, our analysis indicates that a majority of the reactivity and current distribution in GDEs for CO_2R occur at a double-phase boundary and not a triple-phase boundary, contrary to what the majority of literature reports.

AUTHOR INFORMATION

Corresponding Author

*E-mail: nathan.nesbitt@gmail.com, Wilson.Smith@NREL.gov.

Author Contributions

The manuscript was written through contributions of all authors. All authors have given approval to the final version of the manuscript.

ASSOCIATED CONTENT

Supporting Information.

The following files are available free of charge. Supporting Figure S1 showing different cell architectures, Supporting Figure S2 showing capillary pressure vs. pore size, Supporting Figure S3 showing the topography and current of ethylene producing GDEs, a summary of DFT and MD simulations of CO_2 at a gas-liquid boundary with corresponding Supporting Figure S4, the model used for surface diffusion of CO_2, Supporting Figure S5 showing an electrolyte meniscus on Pt and the HOR current through it, and Supporting Table S1 showing values of parameters used in surface diffusion transport estimates, (PDF)

ACKNOWLEDGMENT

This work was authored in part by the National Renewable Energy Laboratory (NREL), operated by Alliance for Sustainable Energy, LLC, for the U.S. Department of Energy (DOE) under Contract No. DE-AC36-08GO$_2$8308. This work was supported by the Laboratory Directed Research and Development (LDRD) Program at NREL. The views expressed in the article do not necessarily represent the views of the DOE or the U.S. Government. The U.S. Government retains and the publisher, by accepting the article for publication, acknowledges that the U.S. Government retains a nonexclusive, paid-up, irrevocable, worldwide license to publish or reproduce the published form of this work, or allow others to do so, for U.S. Government purposes.

Thomas Burdyny acknowledges support of the NWO in the form of a Veni grant.

ABBREVIATIONS

CO_2, carbon dioxide; CO_2R, CO_2 reduction; GDL, gas diffusion layer; GDE, gas diffusion electrodes; STP, standard temperature and pressure; MPL, microporous layer; PTFE, polytetrafluoroethylene; CL, catalyst layer; F.E., Faradaic efficient; TPB, triple-phase boundary; DPB, double-phase boundary; UHV, ultra-high vacuum; b-CO_2, bent CO_2; APXPS, ambient pressure X-ray photoelectron spectroscopy; DFT, density functional theory; MD, molecular dynamics; HOR, hydrogen oxidation reaction; ORR, oxygen reduction reaction.

REFERENCES

(1) Jouny, M.; Luc, W.; Jiao, F. General Techno-Economic Analysis of CO2 Electrolysis Systems. *Ind. Eng. Chem. Res.* **2018**, *57* (6), 2165–2177. https://doi.org/10.1021/acs.iecr.7b03514.

(2) Verma, S.; Kim, B.; Jhong, H.-R. "Molly"; Ma, S.; Kenis, P. J. A. A Gross-Margin Model for Defining Technoeconomic Benchmarks in the Electroreduction of CO2. *ChemSusChem* **2016**, *9* (15), 1972–1979. https://doi.org/10.1002/cssc.201600394.

(3) Smith, W. A.; Burdyny, T.; Vermaas, D. A.; Geerlings, H. Pathways to Industrial-Scale Fuel Out of Thin Air from CO2 Electrolysis. *Joule* **2019**, *3* (8), 1822–1834. https://doi.org/10.1016/j.joule.2019.07.009.

(4) Hori, Y. Electrochemical CO2 Reduction on Metal Electrodes. In *Modern Aspects of Electrochemistry*; Vayenas, C. G., White, R. E., Gamboa-Aldeco, M. E., Eds.; Modern Aspects of Electrochemistry; Springer New York: New York, NY, 2008; Vol. 42, pp 89–189. https://doi.org/10.1007/978-0-387-49489-0_3.

(5) Burdyny, T.; A. Smith, W. CO 2 Reduction on Gas-Diffusion Electrodes and Why Catalytic Performance Must Be Assessed at Commercially-Relevant Conditions. *Energy Environ. Sci.* **2019**, *12* (5), 1442–1453. https://doi.org/10.1039/C8EE03134G.

(6) Wu, K.; Birgersson, E.; Kim, B.; Kenis, P. J. A.; Karimi, I. A. Modeling and Experimental Validation of Electrochemical Reduction of CO2 to CO in a Microfluidic Cell. *J. Electrochem. Soc.* **2014**, *162* (1), F23–F32. https://doi.org/10.1149/2.1021414jes.

(7) Dinh, C.-T.; Burdyny, T.; Kibria, M. G.; Seifitokaldani, A.; Gabardo, C. M.; García de Arquer, F. P.; Kiani, A.; Edwards, J. P.; De Luna, P.; Bushuyev, O. S.; Zou, C.; Quintero-Bermudez, R.; Pang, Y.; Sinton, D.; Sargent, E. H. CO2 Electroreduction to Ethylene via Hydroxide-Mediated Copper Catalysis at an Abrupt Interface. *Science* **2018**, *360* (6390), 783–787. https://doi.org/10.1126/science.aas9100.

(8) Reyes, A.; Jansonius, R. P.; Mowbray, B. A. W.; Cao, Y.; Wheeler, D. G.; Chau, J.; Dvorak, D. J.; Berlinguette, C. P. Managing Hydration at the Cathode Enables Efficient CO2 Electrolysis at Commercially Relevant Current Densities. *ACS Energy Lett.* **2020**, *5*, 1612–1618. https://doi.org/10.1021/acsenergylett.0c00637.

(9) Li, Y. C.; Zhou, D.; Yan, Z.; Gonçalves, R. H.; Salvatore, D. A.; Berlinguette, C. P.; Mallouk, T. E. Electrolysis of CO2 to Syngas in Bipolar Membrane-Based Electrochemical Cells. *ACS Energy Lett.* **2016**, *1* (6), 1149–1153. https://doi.org/10.1021/acsenergylett.6b00475.
(10) Cook, R. L.; MacDuff, R. C.; Sammells, A. F. High Rate Gas Phase Reductionto Ethylene and Methane Using Gas Diffusion Electrodes. *J. Electrochem. Soc.* **1990**, *137* (2), 607–608.
(11) Ma, S.; Luo, R.; Gold, J. I.; Yu, A. Z.; Kim, B.; Kenis, P. J. A. Carbon Nanotube Containing Ag Catalyst Layers for Efficient and Selective Reduction of Carbon Dioxide. *J. Mater. Chem. A* **2016**, *4*, 8573–8578.
(12) Luo, W.; Zhang, J.; Li, M.; Züttel, A. Boosting CO Production in Electrocatalytic CO2 Reduction on Highly Porous Zn Catalysts. *ACS Catal.* **2019**, *9*, 3783−3791.
(13) García de Arquer, F. P.; Dinh, C.-T.; Ozden, A.; Wicks, J.; McCallum, C.; Kirmani, A. R.; Nam, D.-H.; Gabardo, C.; Seifitokaldani, A.; Wang, X.; Li, Y. C.; Li, F.; Edwards, J.; Richter, L. J.; Thorpe, S. J.; Sinton, D.; Sargent, E. H. CO2 Electrolysis to Multicarbon Products at Activities Greater than 1 A Cm−2. *Science* **2020**, *367* (6478), 661–666. https://doi.org/10.1126/science.aay4217.
(14) Westphal, C. Apparat Zur Erzeugung Elektrischer Ströme. DRP 16, 1880.
(15) Bacon, F. T. The High Pressure Hydrogen-Oxygen Fuel Cell. *FUEL CELLS* **1960**, *52* (4), 301–303.
(16) Austin, L. G.; Ariet, M.; Walker, R. D.; Wood, G. B.; Comyn, R. H. Simple-Pore and Thin-Film Models of Porous Gas Diffusion Electrodes. *Ind. Eng. Chem. Fundamen.* **1965**, *4* (3), 321–327.
(17) Li, J.; Chen, G.; Zhu, Y.; Liang, Z.; Pei, A.; Wu, C.-L.; Wang, H.; Lee, H. R.; Liu, K.; Chu, S.; Cui, Y. Efficient Electrocatalytic CO 2 Reduction on a Three-Phase Interface. *Nat. Catal.* **2018**, *1* (8), 592–600. https://doi.org/10.1038/s41929-018-0108-3.
(18) Li, J.; Chang, K.; Zhang, H.; He, M.; Goddard III, W. A.; Chen, J. G.; Cheng, M.-J.; Lu, Q. Effectively Increased Efficiency for Electroreduction of Carbon Monoxide Using Supported Polycrystalline Copper Powder Electrocatalysts. *ACS Catal.* **2019**, *9*, 4709−4718.
(19) Jouny, M.; Luc, W.; Jiao, F. High-Rate Electroreduction of Carbon Monoxide to Multi-Carbon Products. *Nat. Catal.* **2018**, *1* (10), 748–755. https://doi.org/10.1038/s41929-018-0133-2.
(20) Malkhandi, S.; Yeo, B. S. Electrochemical Conversion of Carbon Dioxide to High Value Chemicals Using Gas-Diffusion Electrodes. *Curr. Opin. Chem. Eng.* **2019**, *26*, 112–121. https://doi.org/10.1016/j.coche.2019.09.008.
(21) She, X.; Zhang, T.; Li, Z.; Li, H.; Xu, H.; Wu, J. Tandem Electrodes for Carbon Dioxide Reduction into C2+ Products at Simultaneously High Production Efficiency and Rate. *Cell Reports Physical Science* **2020**, *1* (4), 100051. https://doi.org/10.1016/j.xcrp.2020.100051.
(22) Möller, T.; Ju, W.; Bagger, A.; Wang, X.; Luo, F.; Thanh, T. N.; Varela, A. S.; Rossmeisl, J.; Strasser, P. Efficient CO2 to CO Electrolysis on Solid Ni–N–C Catalysts at Industrial Current Densities. *Energy Environ. Sci.* **2019**, *12* (2), 640–647. https://doi.org/10.1039/C8EE02662A.
(23) Duarte, M.; De Mot, B.; Hereijgers, J.; Breugelmans, T. Electrochemical Reduction of CO2: Effect of Convective CO2 Supply in Gas Diffusion Electrodes. *ChemElectroChem* **2019**, *6* (22), 5596–5602. https://doi.org/10.1002/celc.201901454.

(24) Leonard, M. E.; Clarke, L. E.; Forner-Cuenca, A.; Brown, S. M.; Brushett, F. R. Investigating Electrode Flooding in a Flowing Electrolyte, Gas-Fed Carbon Dioxide Electrolyzer. *ChemSusChem* **2020**, *13* (2), 400–411. https://doi.org/10.1002/cssc.201902547.
(25) Weng, L.-C.; Bell, A. T.; Weber, A. Z. Modeling Gas-Diffusion Electrodes for CO2 Reduction. *Phys. Chem. Chem. Phys.* **2018**, *20* (25), 16973–16984. https://doi.org/10.1039/C8CP01319E.
(26) Hernandez-Aldave, S.; Andreoli, E. Fundamentals of Gas Diffusion Electrodes and Electrolysers for Carbon Dioxide Utilisation: Challenges and Opportunities. *Catalysts* **2020**, *10* (6), 713. https://doi.org/10.3390/catal10060713.
(27) Ogura, K.; Endo, N. Electrochemical Reduction of CO 2 with a Functional Gas-Diffusion Electrode in Aqueous Solutions With and Without Propylene Carbonate. *J. Electrochem. Soc.* **1999**, *146* (10), 3736–3740. https://doi.org/10.1149/1.1392542.
(28) Yano, H.; Shirai, F.; Nakayama, M.; Ogura, K. Efficient Electrochemical Conversion of CO2 to CO, C2H4 and CH4 at a Three-Phase Interface on a Cu Net Electrode in Acidic Solution. *J. Electroanal. Chem.* **2002**, *519*, 93–100.
(29) Yano, H.; Shirai, F.; Nakayama, M.; Ogura, K. Electrochemical Reduction of CO2 at Three-Phase (Gas j Liquid j Solid) and Two-Phase (Liquid j Solid) Interfaces on Ag Electrodes. *J. Electroanal. Chem.* **2002**, *533*, 113–118.
(30) Mason, J. H.; Celik, I. B.; Abernathy, H.; Hackett, G. A. Modified Butler-Volmer Type Model Which Accounts for Triple and Double Phase Boundary Reaction Pathways. *ECS Trans.* **2017**, *78* (1), 2855. https://doi.org/10.1149/07801.2855ecst.
(31) Horsthemke, A.; Schröder, J. J. The Wettability of Industrial Surfaces: Contact Angle Measurements and Thermodynamic Analysis. *Chem. Eng. Process.,* **1985**, *19* (5), 277–285. https://doi.org/10.1016/0255-2701(85)80020-9.
(32) Zahiri, B.; Sow, P. K.; Kung, C. H.; Mérida, W. Active Control over the Wettability from Superhydrophobic to Superhydrophilic by Electrochemically Altering the Oxidation State in a Low Voltage Range. *Adv. Mater. Interfaces* **2017**, *4* (12), 1700121. https://doi.org/10.1002/admi.201700121.
(33) Gim, S.; Cho, K. J.; Lim, H.-K.; Kim, H. Structure, Dynamics, and Wettability of Water at Metal Interfaces. *Sci. Rep.* **2019**, *9* (1), 14805. https://doi.org/10.1038/s41598-019-51323-5.
(34) Gardner, J. R.; Woods, R. The Hydrophilic Nature of Gold and Platinum. *J. Electroanal. Chem. Interfacial. Electrochem.* **1977**, *81* (2), 285–290. https://doi.org/10.1016/S0022-0728(77)80024-7.
(35) Quéré, D. Wetting and Roughness. *Annu. Rev. Mater. Res.* **2008**, *38* (1), 71–99. https://doi.org/10.1146/annurev.matsci.38.060407.132434.
(36) Dai, X.; Stogin, B. B.; Yang, S.; Wong, T.-S. Slippery Wenzel State. *ACS Nano* **2015**, *9* (9), 9260–9267. https://doi.org/10.1021/acsnano.5b04151.
(37) Liu, K.; Smith, W. A.; Burdyny, T. Introductory Guide to Assembling and Operating Gas Diffusion Electrodes for Electrochemical CO2 Reduction. *ACS Energy Lett.* **2019**, *4* (3), 639–643. https://doi.org/10.1021/acsenergylett.9b00137.
(38) Phillips, R. K.; Friess, B. R.; Hicks, A. D.; Bellerive, J.; Hoorfar, M. Ex-Situ Measurement of Properties of Gas Diffusion Layers of PEM Fuel Cells. *Energy Procedia* **2012**, *29*, 486–495. https://doi.org/10.1016/j.egypro.2012.09.057.

(39) Honschoten, J. W. van; Brunets, N.; Tas, N. R. Capillarity at the Nanoscale. *Chem. Soc. Rev.* **2010**, *39* (3), 1096–1114. https://doi.org/10.1039/B909101G.
(40) McLaughlin, D.; Bierling, M.; Moroni, R.; Vogl, C.; Schmid, G.; Thiele, S. Tomographic Reconstruction and Analysis of a Silver CO2 Reduction Cathode. *Adv. Energy Mater.* **2020**, 2000488. https://doi.org/10.1002/aenm.202000488.
(41) Shi, R.; Guo, J.; Zhang, X.; Waterhouse, G. I. N.; Han, Z.; Zhao, Y.; Shang, L.; Zhou, C.; Jiang, L.; Zhang, T. Efficient Wettability-Controlled Electroreduction of CO 2 to CO at Au/C Interfaces. *Nat. Commun.* **2020**, *11* (1), 3028. https://doi.org/10.1038/s41467-020-16847-9.
(42) Wakerley, D.; Lamaison, S.; Ozanam, F.; Menguy, N.; Mercier, D.; Marcus, P.; Fontecave, M.; Mougel, V. Bio-Inspired Hydrophobicity Promotes CO 2 Reduction on a Cu Surface. *Nat. Mater.* **2019**, *18* (11), 1222–1227. https://doi.org/10.1038/s41563-019-0445-x.
(43) Chizmadzhev, Yu. A.; Chirkov, Yu. G. In *Comprehensive Treatise of Electrochemistry: Electrodics: Transport.*; ed. E. Yeager, J. O'M. Bockris, B. E. Conway, S. Sarangapani, Springer: New York, NY, 1983, ch. 5, pp. 317-392.
(44) Jhong, H.-R. "Molly"; Brushett, F. R.; Kenis, P. J. A. Fuel Cells: The Effects of Catalyst Layer Deposition Methodology on Electrode Performance (Adv. Energy Mater. 5/2013). *Adv. Energy Mater.* **2013**, *3* (5), 541–541. https://doi.org/10.1002/aenm.201370019.
(45) De Gregorio, G. L.; Burdyny, T.; Loiudice, A.; Iyengar, P.; Smith, W. A.; Buonsanti, R. Facet-Dependent Selectivity of Cu Catalysts in Electrochemical CO2 Reduction at Commercially Viable Current Densities. *ACS Catal.* **2020**, *10* (9), 4854–4862. https://doi.org/10.1021/acscatal.0c00297.
(46) Dufek, E. J.; Lister, T. E.; McIlwain, M. E. Bench-Scale Electrochemical System for Generation of CO and Syn-Gas. *J Appl Electrochem* **2011**, *41* (6), 623–631. https://doi.org/10.1007/s10800-011-0271-6.
(47) Duan, Q.; Wang, H.; Benziger, J. Transport of Liquid Water through Nafion Membranes. *J. Membr. Sci.* **2012**, *392–393*, 88–94. https://doi.org/10.1016/j.memsci.2011.12.004.
(48) Kusoglu, A.; Weber, A. Z. New Insights into Perfluorinated Sulfonic-Acid Ionomers. *Chem. Rev.* **2017**, *117* (3), 987–1104. https://doi.org/10.1021/acs.chemrev.6b00159.
(49) Li, X.; Feng, F.; Zhang, K.; Ye, S.; Kwok, D. Y.; Birss, V. Wettability of Nafion and Nafion/Vulcan Carbon Composite Films. *Langmuir* **2012**, *28* (16), 6698–6705. https://doi.org/10.1021/la300388x.
(50) Goswami, S.; Klaus, S.; Benziger, J. Wetting and Absorption of Water Drops on Nafion Films. *Langmuir* **2008**, *24* (16), 8627–8633. https://doi.org/10.1021/la800799a.
(51) Somasundaram, T.; Lynden-Bell, R. M.; Patterson, C. H. The Passage of Gases through the Liquid Water/Vapour Interface: A Simulation Study. *Phys. Chem. Chem. Phys.* **1999**, *1* (1), 143–148. https://doi.org/10.1039/A805067H.
(52) Zhang, H.; Singer, S. J. Analysis of the Subcritical Carbon Dioxide-Water Interface. *J. Phys. Chem. A* **2011**, *115*, 6285–6296.
(53) Solymosi, F. The Bonding, Structure and Reactions of CO2 Adsorbed on Clean and Promoted Metal Surfaces. *J. Mol. Catal.* **1991**, *65* (3), 337–358. https://doi.org/10.1016/0304-5102(91)85070-I.
(54) Freund, H.-J.; Roberts, M. W. Surface Chemistry of Carbon Dioxide. *Surf. Sci. Rep.* **1996**, *25* (8), 225–273. https://doi.org/10.1016/S0167-5729(96)00007-6.

(55) Ernst, K.-H.; Schlatterbeck, D.; Christmann, K. Adsorption of Carbon Dioxide on Cu(110) and on Hydrogen and Oxygen Covered Cu(110) Surfaces. *Phys. Chem. Chem. Phys.* **1999**, *1* (17), 4105–4112. https://doi.org/10.1039/a904169i.

(56) Davies, P. R.; Keel, J. M. The Reaction of Carbon Dioxide with Amines at a Cu(211) Surface. *Surf. Sci.* **2000**, *469* (2), 204–213. https://doi.org/10.1016/S0039-6028(00)00827-X.

(57) Burghaus, U. Surface Chemistry of CO2 – Adsorption of Carbon Dioxide on Clean Surfaces at Ultrahigh Vacuum. *Prog. Surf. Sci.* **2014**, *89* (2), 161–217. https://doi.org/10.1016/j.progsurf.2014.03.002.

(58) Ye, Y.; Yang, H.; Qian, J.; Su, H.; Lee, K.-J.; Cheng, T.; Xiao, H.; Yano, J.; Goddard III, W. A.; Crumlin, E. J. Dramatic Differences in Carbon Dioxide Adsorption and Initial Steps of Reduction between Silver and Copper. *Nat. Commun.* **2019**, *10* (1), 1875. https://doi.org/10.1038/s41467-019-09846-y.

(59) Favaro, M.; Xiao, H.; Cheng, T.; Goddard III, W. A.; Yano, J.; Crumlin, E. J. Subsurface Oxide Plays a Critical Role in CO2 Activation by Cu(111) Surfaces to Form Chemisorbed CO2, the First Step in Reduction of CO2. *Proc. Natl. Acad. Sci. U.S.A.* **2017**, *114* (26), 6706–6711. https://doi.org/10.1073/pnas.1701405114.

(60) J. Firet, N.; A. Blommaert, M.; Burdyny, T.; Venugopal, A.; Bohra, D.; Longo, A.; A. Smith, W. Operando EXAFS Study Reveals Presence of Oxygen in Oxide-Derived Silver Catalysts for Electrochemical CO 2 Reduction. *J. Mater. Chem. A* **2019**, *7* (6), 2597–2607. https://doi.org/10.1039/C8TA10412C.

(61) Mistry, H.; Choi, Y.-W.; Bagger, A.; Scholten, F.; Bonifacio, C. S.; Sinev, I.; Divins, N. J.; Zegkinoglou, I.; Jeon, H. S.; Kisslinger, K.; Stach, E. A.; Yang, J. C.; Rossmeisl, J.; Roldan Cuenya, B. Enhanced Carbon Dioxide Electroreduction to Carbon Monoxide over Defect-Rich Plasma-Activated Silver Catalysts. *Angew. Chem. Int.* **2017**, *129* (38), 11552–11556. https://doi.org/10.1002/ange.201704613.

(62) Meixner, D. L.; Arthur, D. A.; George, S. M. Kinetics of Desorption, Adsorption, and Surface Diffusion of CO2 on MgO(100). *Surf. Sci.* **1992**, *261* (1), 141–154. https://doi.org/10.1016/0039-6028(92)90226-V.

(63) Czanderna, A. W.; Biegen, J. R. Activation Energy for the Desorption of Carbon Dioxide from Oxygen-Covered Silver. *Journal of Vacuum Science and Technology* **1971**, *8* (4), 594–598. https://doi.org/10.1116/1.1315208.

(64) Sladek, K. J.; Gilliland, E. R.; Baddour, R. F. Diffusion on Surfaces. II. Correlation of Diffusivities of Physically and Chemically Adsorbed Species. *Ind. Eng. Chem. Fund.* **1974**, *13* (2), 100–105. https://doi.org/10.1021/i160050a002.

(65) Moultos, O. A.; Tsimpanogiannis, I. N.; Panagiotopoulos, A. Z.; Economou, I. G. Atomistic Molecular Dynamics Simulations of CO2 Diffusivity in H2O for a Wide Range of Temperatures and Pressures. *J. Phys. Chem. B* **2014**, *118* (20), 5532–5541. https://doi.org/10.1021/jp502380r.

(66) Tao, G. Nonadiabatic Dynamics of Hydrogen Diffusion on Cu(001): Classical Mapping Model with Multistate Projection Window in Real Space. *ChemPhysChem* **2019**, *20* (16), 2127–2135. https://doi.org/10.1002/cphc.201900296.

(67) Xu, L.; Lin, J.; Bai, Y.; Mavrikakis, M. Atomic and Molecular Adsorption on Cu(111). *Top. Catal.* **2018**, *61* (9), 736–750. https://doi.org/10.1007/s11244-018-0943-0.

(68) Tabatabaei, J.; Sakakini, B. H.; Watson, M. J.; Waugh, K. C. The Detailed Kinetics of the Desorption of Hydrogen from Polycrystalline Copper Catalysts. *Catal. Lett.* **1999**, *59* (2), 143–149. https://doi.org/10.1023/A:1019080823616.
(69) Somasundaram, T.; in het Panhuis, M.; Lynden-Bell, R. M.; Patterson, C. H. A Simulation Study of the Kinetics of Passage of CO2 and N2 through the Liquid/Vapor Interface of Water. *J. Chem. Phys.* **1999**, *111* (5), 2190–2199.
(70) Balej, J. Water Vapour Partial Pressures and Water Activities in Potassium and Sodium Hydroxide Solutions over Wide Concentration and Temperature Ranges. *Int. J. Hydrogen Energy* **1985**, *10* (4), 233–243. https://doi.org/10.1016/0360-3199(85)90093-X.
(71) Åkerlöf, G.; Kegeles, G. Thermodynamics of Concentrated Aqueous Solutions of Sodium Hydroxide1,2. **1940**, *62*, 620–640.
(72) Ooka, H.; Figueiredo, M. C.; Koper, M. T. M. Competition between Hydrogen Evolution and Carbon Dioxide Reduction on Copper Electrodes in Mildly Acidic Media. *Langmuir* **2017**, *33* (37), 9307–9313. https://doi.org/10.1021/acs.langmuir.7b00696.
(73) Yang, K.; Kas, R.; Smith, W. A. In Situ Infrared Spectroscopy Reveals Persistent Alkalinity near Electrode Surfaces during CO2 Electroreduction. *J. Am. Chem. Soc.* **2019**, *141* (40), 15891–15900. https://doi.org/10.1021/jacs.9b07000.
(74) Rosen, J.; Hutchings, G. S.; Lu, Q.; Rivera, S.; Zhou, Y.; Vlachos, D. G.; Jiao, F. Mechanistic Insights into the Electrochemical Reduction of CO2 to CO on Nanostructured Ag Surfaces. *ACS Catal.* **2015**, *5* (7), 4293–4299. https://doi.org/10.1021/acscatal.5b00840.
(75) Dunwell, M.; Luc, W.; Yan, Y.; Jiao, F.; Xu, B. Understanding Surface-Mediated Electrochemical Reactions: CO2 Reduction and Beyond. *ACS Catal.* **2018**, *8* (9), 8121–8129. https://doi.org/10.1021/acscatal.8b02181.
(76) O'M. Bockris, J.; Cahan, B. D. Effect of a Finite-Contact-Angle Meniscus on Kinetics in Porous Electrode Systems. *J. Chem. Phys.* **1969**, *50* (3), 1307–1324. https://doi.org/10.1063/1.1671193.
(77) Gileadi, E. *Electrode Kinetics for Chemists, Chemical Engineers and Materials Scientists*; pages 484-487. Wiley-VCH: Berlin, Germany, 1993.
(78) Woo, A. L.-W. Conductance Studies of Concentrated Solutions of Sodium Hydroxide and Potassium Hydroxide Electrolytes, page 39. South Dakota State University, 1968.
(79) Ma, M.; Clark, E. L.; Therkildsen, K. T.; Dalsgaard, S.; Chorkendorff, I.; Seger, B. Insights into the Carbon Balance for CO2 Electroreduction on Cu Using Gas Diffusion Electrode Reactor Designs. *Energy Environ. Sci.* **2020**, *13* (3), 977–985. https://doi.org/10.1039/D0EE00047G.
(80) Verma, S.; Lu, X.; Ma, S.; Masel, R. I.; Kenis, P. J. A. The Effect of Electrolyte Composition on the Electroreduction of CO2 to CO on Ag Based Gas Diffusion Electrodes. *Phys. Chem. Chem. Phys.* **2016**, *18* (10), 7075–7084. https://doi.org/10.1039/C5CP05665A.
(81) Röhe, M.; Botz, A.; Franzen, D.; Kubannek, F.; Ellendorff, B.; Öhl, D.; Schuhmann, W.; Turek, T.; Krewer, U. The Key Role of Water Activity for the Operating Behavior and Dynamics of Oxygen Depolarized Cathodes. *ChemElectroChem* **2019**, *6* (22), 5671–5681. https://doi.org/10.1002/celc.201901224.
(82) Hitchcock, L. B. Rate of Absorption of Carbon Dioxide Effect of Concentration and Viscosity of Caustic Solutions. *Ind. Eng. Chem.* **1934**, *26* (11), 1158–1167.

(83) Han, X.; Yu, Z.; Qu, J.; Qi, T.; Guo, W.; Zhang, G. Measurement and Correlation of Solubility Data for CO2 in NaHCO3 Aqueous Solution. *J. Chem. Eng. Data* **2011**, *56* (4), 1213–1219. https://doi.org/10.1021/je1011168.
(84) Ma, S.; Odgaard, M.; Skou, E. Carbon Dioxide Permeability of Proton Exchange Membranes for Fuel Cells. *Solid State Ionics* **2005**, *176* (39), 2923–2927. https://doi.org/10.1016/j.ssi.2005.09.024.
(85) Paulisch, M. C.; Gebhard, M.; Franzen, D.; Hilger, A.; Osenberg, M.; Kardjilov, N.; Ellendorff, B.; Turek, T.; Roth, C.; Manke, I. Operando Laboratory X-Ray Imaging of Silver-Based Gas Diffusion Electrodes during Oxygen Reduction Reaction in Highly Alkaline Media. *Materials* **2019**, *12* (17), 2686. https://doi.org/10.3390/ma12172686.
(86) Normile, S. J.; Sabarirajan, D. C.; Calzada, O.; De Andrade, V.; Xiao, X.; Mandal, P.; Parkinson, D. Y.; Serov, A.; Atanassov, P.; Zenyuk, I. V. Direct Observations of Liquid Water Formation at Nano- and Micro-Scale in Platinum Group Metal-Free Electrodes by Operando X-Ray Computed Tomography. *Materials Today Energy* **2018**, *9*, 187–197. https://doi.org/10.1016/j.mtener.2018.05.011.